

Microstructural Analysis of a Girth Welded Subsea Pipe

Bridget E. Kogo, Bin Wang, Luiz C. Wrobel and Mahmoud Chizari, *Member IAENG*

Abstract—This research focuses on simulation of the dissimilar materials' welding, stainless steel and mild steel, using finite element and experiment to enhance the method and better understand the transient temperature profiles and the stress distribution in a clad pipe. The microstructural come as fenestrated and the computer results show that the temperature distribution in the modelled pipe is a function of the thermal conductivity of each weld metal as well as the distance away from the heat source.

Index Terms—Transient temperature response, dissimilar material joint, girth weld, microstructure

I. INTRODUCTION

IT is known that the welding of cylindrical objects is complex and poses a source of concern in manufacturing processes. There are several benefits of welding as a joining technology which includes cost effectiveness, flexibility in design, enhanced structural integrity, and composite weight reduction. However, thermal stresses are usually initiated on the weld and the base metal [1-5]. Poorly welded joints result in leakages, pipe failures and bursts, which lead to possible environmental hazards, loss of lives and properties. Welding of dissimilar materials is carried out in-house using Gas Metal Arc Weld (GMAW), and a finite element analysis (FEA) on pipe models having different clad thicknesses of 2mm and 12mm, respectively, and the temperature versus distance profile obtained. The 12mm clad pipe results are discussed in this paper.

The process of carrying out welding using an arc weld entails melting down the base metal and, in this research, it also involves melting down the clad metal. In the course of carrying out the welding, filler metals are also melted such that the solution formed by heating up all these materials and holding them at that range of temperature long enough permits the diffusion of constituents into the molten solution; this is followed by cooling down rapidly in order to maintain these constituents within the solution. The result of this procedure generates a metallurgical structure positioning in-situ the material which supplies superior tensile strength. The bulk of the material immediately after the fusion zone (FZ), which has its characteristics altered by the weld, is termed Heat Affected Zone (HAZ). The volume of material within the HAZ undergoes considerable change which could be

advantageous to the weld joint, but in some circumstances, might not be beneficial. The aim of this paper is to closely look at welding of dissimilar materials and compare the results with the computer modelling of different cladding thickness.

II. FE ANALYSIS

The underlying theory behind weld research is based on the Gaussian transformation principle, which states that 'A Gaussian flat surface has a Gaussian curvature at each and every point of the magnitude of zero'. Going by this principle, the surface of a cylinder can be said to be a Gaussian flat plane since it can be revolved from a piece of paper. Furthermore, the implication is that this can be done without stretching the plane, folding or tearing it [6]. This means that the thermal distributions on the surface of a cylinder can also be appreciated by studying the thermal distribution on the surface of welded plates.

For the clad pipe, shown in Figure 1, the total number of nodes in the FEA mesh is 208,640 and elements 180,306. An 8-node linear brick is generated using a hexagonal element. Linear hexahedral elements are recommended for their reduced computation time and ease of running analysis due to the structured grid which makes up the mesh. All elements are identical on this structured array. Hexahedral elements guarantee minimal skewness because of their uniform grid shape; however, a hexahedral mesh can also be unstructured depending on the manner in which element indexing is executed [7].

III. FINITE ELEMENT MODELS

A thermal simulation for heat pass 1 in a full 3D pipe has been shown in Figure 1. The temperature contours, which are seen as colour variations, representing each thermal distribution shown in the temperature panel on the top left-hand side of the figure. The red band depicts the hottest part of the weld with a temperature of 1,545°C, whereas the other regions are depicted by a lower temperature leaving the bulk of the pipe at 99°C. The FZ corresponds to temperatures between 1,304°C to 1,545°C and is depicted by the orange-reddish band, whereas the HAZ is represented by the yellowish greenish blue bands and ranges from 220°C to 1,184°C.

Manuscript received Feb 15, 2017; revised January 17, 2018.

Bridget E. Kogo (corresponding author) is with Mechanical, Aerospace and Civil Engineering Department, College of Engineering, Design and Physical Sciences, Brunel University London, UK (e-mail: biddyagada@yahoo.com)

Bin Wang is with Mechanical, Aerospace and Civil Engineering Department, College of Engineering, Design and Physical Sciences, Brunel University London, UK (e-mail: bin.wang@brunel.ac.uk)

Luiz C. Wrobel is with Mechanical, Aerospace and Civil Engineering Department, College of Engineering, Design and Physical Sciences, Brunel University London, UK (e-mail: luiz.wrobel@brunel.ac.uk)

Mahmoud Chizari is with the School of Mechanical Engineering, Sharif University of Technology in Tehran. He is also with Mechanical, Aerospace and Civil Engineering Department, College of Engineering, Design and Physical Sciences, Brunel University London, Uxbridge, UB8 3PH, UK (e-mail: mahmoudchizari@yahoo.com)

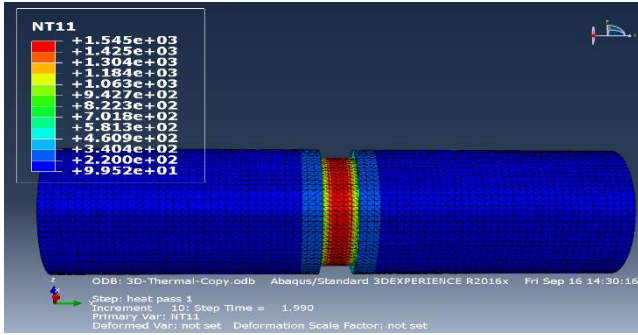


Fig. 1. A 3D model showing the different weld profiles for heat pass 1. Temperature profiles of a ring weld through the weld pass length.

IV. TENSILE TEST

Several factors such as temperature, strain rate and anisotropy affect the shape of the stress-strain curves. The parent metals have different elongation characteristics, and each exhibit this at different rates because of the applied stress under which it is stretched. Similarly, the behaviour of the weld metal under the displacement curve is also due to slip, which is caused by the elongation and failure of the different metals (mild steel and stainless steel) present within the weld samples, since they each have their original ultimate tensile stress (UTS). The volumetric change and yield strength in Figure 2 as a result of martensitic transformation have influences on the welding residual stresses, increasing the magnitude of the residual stress in the weld zone as well as changing its sign.

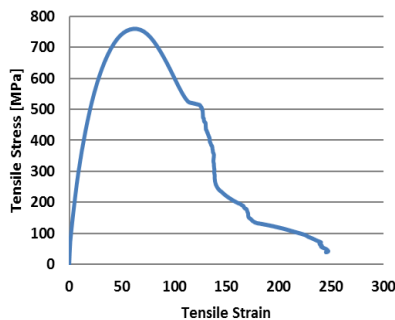


Fig. 2. Stress-strain curve of 12mm clad pipe

V. ELECTRON MICROSCOPY TEST

1) Sample Preparation

1. Two different samples of weld, with the dimensions as shown in Figure 5, were cut from the main weld. The samples each of the parent material: 12mm stainless steel and 10mm mild steel were cut into dimensions: 40mm x 20mm and 20mm.

2. The parent material samples were formed into a mould using 5 spoonful or 2.5 spoonful of Bakelite S and Struers mount press (CitoPress-1 S/N 5770041); to enable easy and controlled grinding. [8] Place sample down on the holder, pour Bakelite unto sample and start. After five mins, mount press heats up for 3 minutes and cools down for two mins. Use the electric scribing tool to label sample.

3. Grinding of samples with manual or automated grinder and silicon carbide papers - The samples were grinded using a grinding machine and different silicon carbide papers from 80, 120, 350, 800, 1200 and 1600. Polishing each time in the opposite direction to the scratches to eliminate the

scratches. Polishing was done in an alternating vertical and horizontal direction for each carbon paper changed.

4. Polishing samples with a polishing cloth.

5. Both hand polishing and machine were carried out.

The sample preparation is like that for SEM and is explained below:

Polishing weld samples with of varying degree of polish paper (carbide). At each stage, the sample was washed clean with water and surface preserved (to avoid oxidation) with ethanol or methanol before drying. In the case of washing with methanol, protective breathing, eyes and hand clothing such as gloves eyeglasses were worn for safety of personnel. The sample is then examined under electron microscope to see if the required microstructure has been achieved otherwise polishing continues.

After a mirror surface is achieved, the diamond paste and Colloidal Silica Suspension also called Oxidizing Polishing cloth was used. Rinsing the surface with nitric acid to clean surface and especially preserve from corrosion.

VI. RESULTS AND DISCUSSION

The polishing made the heat affected zone and weld zone visible as shown in the figure below; however, the unique features in the weld zone and heat affected zones were appreciated after etching as shown in Figure 3.

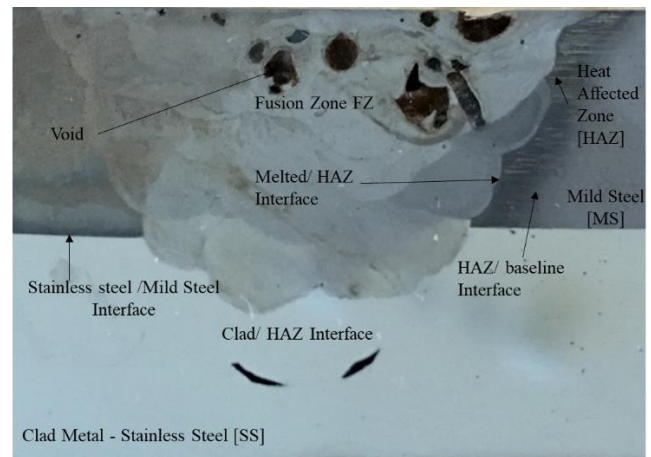


Fig. 3. Micrograph of FZ, HAZ and stainless steel-clad metal

The experiment was carried out in agreement with the standard for grinding and polishing stainless steel cladding with Mild steel [9] [10]. These clad samples were examined with the aid of an optical microscope to observe the microstructural evolutions within the heat affected zone. The heat affected zone is as shown in the Figure 3 and 4. The Heat affected zone is the boundary or zone surrounding the welded zone. This area is of paramount interest in this research because of the grain size formed as well as the constituent elements that make up that zone. Most especially because the large grain formed in this zone as a result of austenitic cooling of the martensitic grains get oxidized when the pipe is laid on the sea bed or in deep offshore operations. As this layer gets eroded, they expose the layer of the clad pipe beneath resulting in pitting. Pitting if not handled properly as result of the pressure of fluid within the pipe and the forces acting on the pipe from surrounding environment, the ocean current also contributing, could lead to a leak, which could result in a burst until there is complete failure of the pipeline.

1) *Vickers hardness test*

Using the Vickers hardness machine, a diamond stud pattern was created with the aid of the pyramidal diamond indenter following strictly the pattern in Figure 4 across the Heat affected and fusion zone and region close to the welded zones of the welded metals. These were repeated in the second and third lines as seen both in the welded sample and the chart. Alternatively, there is the vertical array of similar type of pattern across the HAZ.

The length of the diagonals of the diamond stud was measured both in the vertical (D1) and horizontal (D2) axes and the average reading recorded. This average value of the distance was imputed into a standard equation known as the Vickers Hardness equation as shown below.

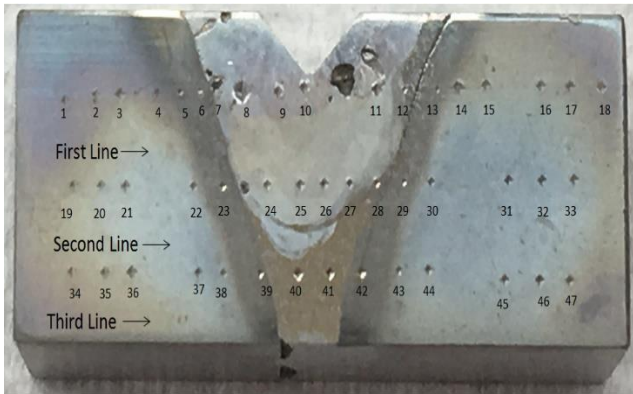
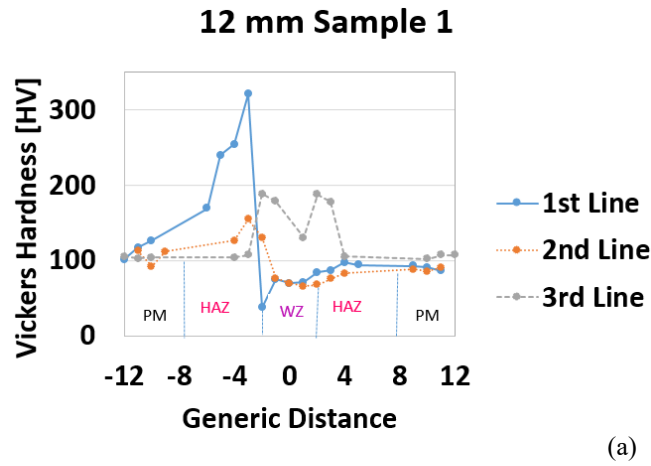
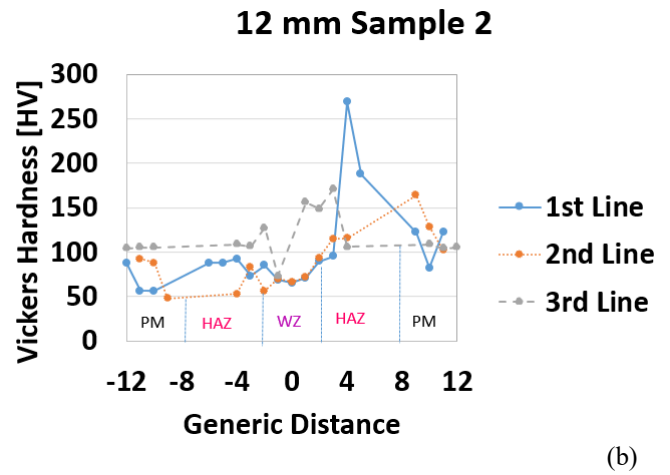


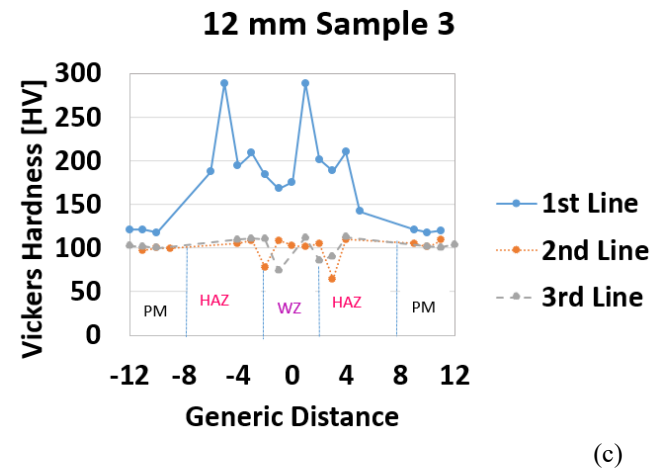
Fig. 4. Pattern and order for diamond stud imprints across HAZ and fusion zones



(a)



(b)



(c)

Fig. 5. A typical electronic microscopy test for 3 different 12mm clad specimens.

It is observed that for the first line of all the 12mm samples 1 to 3 that the hardness is very high in both HAZ and FZ compared with the parent material as shown in Figure 5 (a-c). The peak values of hardness in Figure 5 (a) from left to right are 330 HV at -4, 100 HV at 1; (b) 270 HV at 4, 190 HV at 5 and (c) has 180 HV at 6, 290 HV at 5, 195 HV at 4, 210 HV at 3, 290 HV at 1, 200 HV at 2 and 210 HV at 4. For the second line of the 12mm sample 1 and 2, of Figure 5, the hardness is higher in the HAZ than other regions.

Of significance, is the fact that hardness is also high in the FZ and HAZ of the third line of 12mm samples 1 and 2 in Figure 5 (a-b). This can be seen in Figures 5 (a and b) reading respectively from left to right, (a) has 100 HV at -4, 190 HV at -2, 170 HV at -1, 130 HV at 1, 180 HV at 2, 170 at 3 and 100 HV occurring at 4 likewise; (b) has the following hardness peaks 100 HV at -4, 130 HV at -2, 160 HV at 1, 150 HV at 2, 170 HV at 3 and 100 HV at 4.

From the chart in Figure 5, there is a unique trend in the increased hardness profile across the fusion zone and HAZ of 3rd line in the 12mm samples 1 and 2.

From the Vickers hardness test, it is obvious that the weld hardness is 30% - 70% greater than the parents' metal. This is due to the very high rate of Martensite formation during rapid cooling of the melt pool. Throughout the weld process, there is continuous reheating taking place as the weld touch passes to and from the weld metals. The average hardness of the dilution zone is comparable to that of the clad.

From the hardness plot it is obvious that the hardness of the HAZ varies linearly from the clad/HAZ interface to the HAZ/baseline interface with values 200Hv to 330Hv accordingly. The reason for the direct variation of hardness in the HAZ is the difference in heating temperature in the HAZ resulting in variation in the growth of grain.

The result of the above is the formation of coarse grain because of tall peak temperatures leading to coarser microstructure formed close to the Clad/HAZ interface. On the other hand, finer grain sizes are formed because of subsiding heating temperatures away from the clad/HAZ interface. On the overall, a finer grain size is harder than a coarse grain size.

The HAZ increases proportionately to 330 HV which is typical of the hardness observed during heat treatment ranging from 710°C to 170°C. When A1 is attained in the temperature range, there is a sharp fall in the hardness at the end of the HAZ which implies that there are no γ transformations occurring.

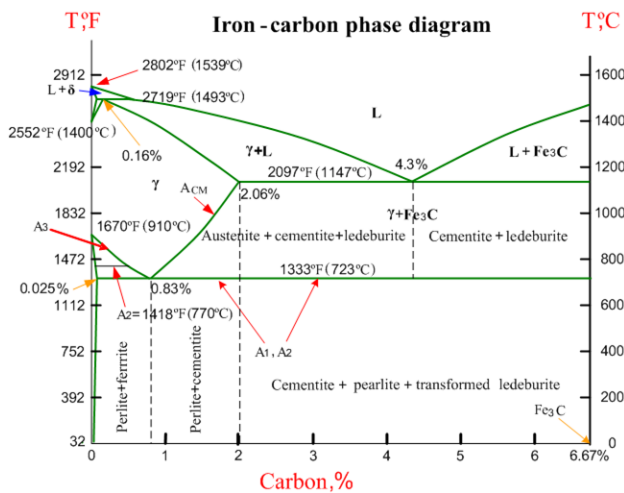


Fig. 6. Phase diagram showing the position of A1[11]

Mechanical properties are relevant to pressure vessels and increase in temperature or increase in irradiation dose increases the yield stress and ultimate tensile stress. This has been experimentally proven [12] and the advantage of this experimentally derived correlation shows that both hardness test and tensile tests were carried out at same temperature which is room temperature, sodium transformed surfaces were removed before micro-hardness test and as many indentations as could be were punched into the metallic surfaces. Experimental studies carried out on larger scale did not factor in the slightest change in composition and possible deposition of ferrite onto the surfaces. Another possibility is also that the brittle nature of the stainless steel at elevated hardening levels could be due to martensitic distortion while carrying out micro hardness dimensions of the low alloy steel [13]. This universal correlation enables the determination of yield stress from the micro hardness value hence improving labour efficiency, see Table I.

Ductile to Brittle Transition Temperature (DBTT) varies in dissimilar materials, some being severe than other; which can be accounted for via a temperature sensitive deformation process. The procedure and behaviour of a Body Centred Cubic (BCC) lattice is triggered by temperature and responds

to reshuffling of the dislocation core just before slip. This could result in challenges for ferritic steel in building of ships. Neutron radiation also influences DBTT, which deforms the internal lattice hence reducing ductility and increasing DBTT.

TABLE I. HARDNESS VS. YIELD STRESS

Specimen	H_V [MPa]	Yield Stress [MPa] = [3.55HV]
12mm Sample 1	320	1136
12mm Sample 2	269	954.95
12mm Sample 3	288	1022.4

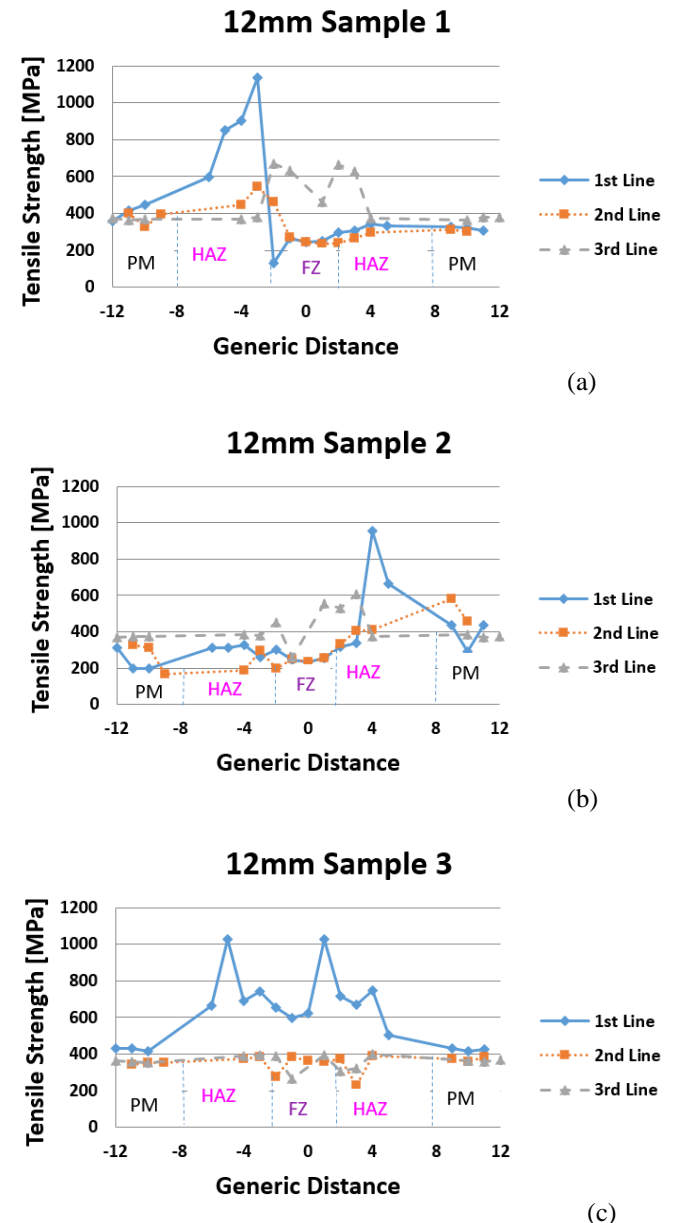


Fig. 7. Plots of yield stress vs hardness for (a) sample 1; (b) sample 2; (c) sample 3. The hardness unit is MPa.

From the plot in Figures 7 (a-c), it further shows a linear relationship exists between the Yield stress and the Hardness of the weld samples which further confirm for the 12mm stainless steel clad that the value of hardness increases with the decrease in temperature and applied load.

There is a similar trend in the increased tensile profile across the fusion zone and HAZ of third line in 12mm

samples 1 and 2 as shown in Figures 7 (a and b) respectively. The values of the peak tensile strength in Figure 7 a) is 668 MPa at -2 and 664.26 MPa at 2 whereas b) has 452.59 MPa at -2, 553.83 MPa at 1 and 606.16 MPa at 3 respectively.

The strength is also high in the Fusion zone and HAZ of the second line for the 12mm sample one and two of figures 7 (a and b). For the 12mm sample one and two, of Figures 7 (a and b) respectively, the strength is higher in the HAZ than other regions.

It is observed that for the first line of all the 12mm samples 1 to 3, the yield strength and consequently the Ultimate Tensile Strength (UTS) is very high at both HAZ and FZ compared with the parents' material as shown in Figures 7 (a-c) respectively.

High thermal gradients were experienced during the Butt welding procedure leading to residual stress and discrepancy in hardness. [14] [15] [16] [17] [18] Because of the high concentration of thermal stress in the clad, the presence of residual stresses usually affects the inherent resistance to corrosion and fatigue cracks. To improve the mechanical properties of the clad/base metal interface, as well as reduce the residual stresses generated, post heat treatments are carried out.

2) Microstructures

From the result obtained in the experiment [19], it is evident that there is an element of carbon in the stainless steel. It was observed from the microstructure [19] that the parent metals - Stainless Steel and Mild Steel - as well as the weld in between contain several elements. Table I reveals the elements present in both stainless steel and mild steel. The Fe content is higher in the mild steel than in the stainless steel. The Nickel content is very high in the stainless steel and absent in the mild steel. Likewise, the Molybdenum content is higher in the stainless steel than in the mild steel. The Cr content is very high in the stainless steel compared with the mild steel [20].

TABLE II. ELEMENTS IN WELD STEEL OF 12mm SS/MS CLAD

Element	Fe	C	Cr	N	Mn	Si	Ca	Mo
SS	71.30	5.08	13.41	7.05	1.51	0.41	0.08	1.16
MS	92.02	5.51	0.61	-	1.13	0.41	0.07	0.25

It is known in welding that the weakest point of the weld is the clad/HAZ interface due to inconsistent fusion and reheating [21]. During Butt welding, there are high thermal gradients experienced during the procedure leading to residual stress and discrepancy in hardness. The presence of residual stresses as a result of high concentration of thermal stress in the clad usually affects the inherent resistance to corrosion and fatigue cracks. In order to enhance the mechanical properties of the clad/base metal interface, as well as reduce the residual stresses generated, post-heat treatments are usually carried out.

The presence of Nickel and Manganese in steel decreases the eutectoid temperature lowering the kinetic barrier whereas Tungsten raises the kinetic barriers. The presence of Manganese increases hardness in steel and likewise Molybdenum.

Within the transition zone next to the weld metal, the stainless-steel part of the microstructures contains acicular

ferrites, which are formed when the cooling rate is high in a melting metal surface or material boundaries. Different ferrites are formed starting from the grain boundary. Such ferrites include plate and lath Martensite, Widmanstatten ferrite, and grain boundary ferrite [22]

VII. XRD ANALYSIS

X-Ray Diffraction is a special process of identifying the degree of structural order of a material. This is crucial because in every atom, there is a unique order of array of the crystals that make up that atom or material and this crystallinity directly affects the density, diffusion hardness or transparency of that material or metal. Since each metal has a peculiar signature,

1) Sample Preparation

The surfaces of the samples were cleansed with ethanol and the weld samples were placed in transparent sample holders; and held in place by plasticine, after which they were placed inside the x-ray detector and the analysis, monitored via the computer as in the figures below shown below. Recall that since welding is a multifaceted process, and different phases are formed by reason of the change in temperatures during the cooling processes; the properties of the weld changes based on the phase changes present in a particular micrograph and sample.

The Bruker AXS Diffraktometer D8 Erz. Nr. 7KP2025-1LG14-3-Z P02, Serial-Nr 203770, (D 76181 Karlsruhe, Germany), was used to analyse the 2mm and 12mm MSSS welded samples and the phase composition as well as the XRD Characterisation was carried out with the aid of the DIFFRAC.EVA software version 4.0 (32 bit) Released in 2014. In order to determine the size occupancy and crystal Structure as well as the angle, Bruker AXS TOPAS version 5 was used to fundamentally compare the structure of the crystals present in these samples with a standard structure of a crystal already existing in the library (since each metal has a peculiar signature), so as to obtain the closest similar characteristics or patterns peculiar to it thereby identifying the structure. Below are found structures of the different phases present within the weld samples.



Fig. 8. 12mm SS/MS Samples prepared for the XRD detector

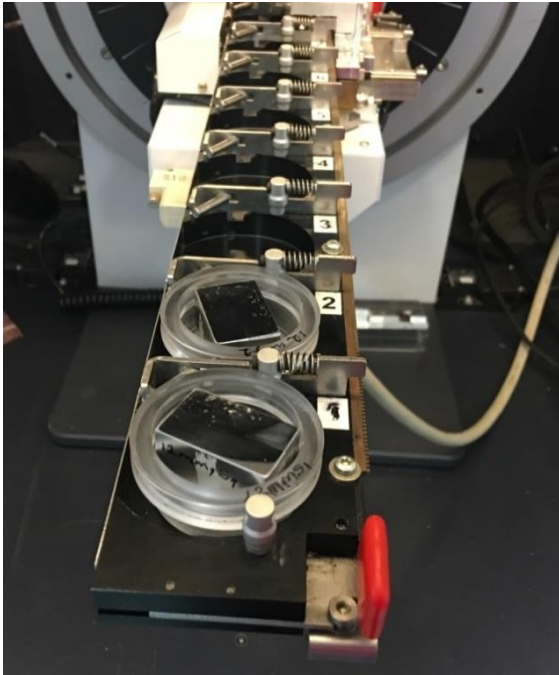


Fig. 9. Array of the 12mm SS/MS Samples on the sample holder of the XRD detector

2) XRD Result

TABLE III PERCENTAGE CRYSTALLINITY AND AMORPHOUS PRESENT IN 2MM MSSS WELD SAMPLES AND % PRESENT IN 12MM MSSS WELD SAMPLES

Samples	%Crystallinity	% Amorphous	Global Area	Reduced Area
12mm MSSS1	9.4	90.6	1269	119.9
12MM MSSS2	50.1	49.9	343.3	172.1

TABLE IV. PHASES PRESENT IN 12MM MSSS WELD SAMPLES AND % QUANTIFICATION PRESENT THE WELD SAMPLES

Samples	Formula	Quantification [%]
12mm MSSS1	Cr _{0.7} Fe _{0.3}	7.4
	Fe ₁₉ Mn α -Fe ₁₉ Mn	6.5
	Fe-Cr ₄ 10L	72.3
	Mn Ni ₃	4.4
	Cr Ni	3.9
	Cr _{0.7} Fe _{0.3} α Cr _{0.7} Fe _{0.3}	5.6
12mm MSSS2	Fe ₃ Ni ₂	53.4
	Fe ₃ Ni ₂	46.6

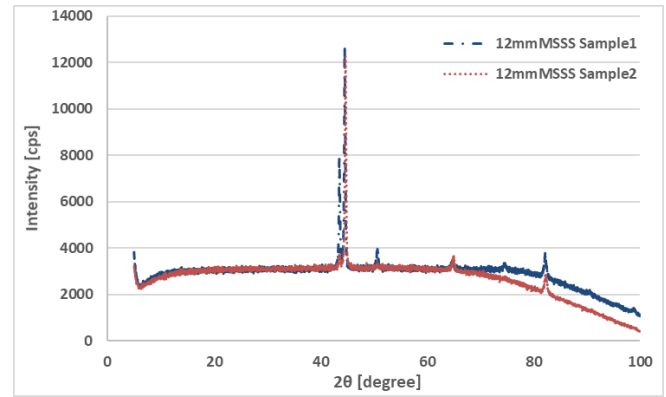


Fig. 10. XRD Pattern for 12mm MSSS (Sample 1) revealing multiphase presence

As a result of the welding martensitic phase was observed in AISI 316 – Cr4. Peaks position shifts towards higher 2θ AISI 316 – Cr4 on comparing with its base metal diffraction, displaying strain produced during welding.

The first Crystal size of Chromium Nickel Phase (the dotted line) in the 12mm MSSS sample 1, is 411.9 Armstrong. This corresponds to the highest peak in the spectrum.

The second Crystal size of Chromium Nickel Phase (the line in dash) in the 12mm MSSS sample 1 is 411.9 Armstrong. This corresponds to the next peak to the right of the spectrum. The detector also detected some quantity of iron manganese and ferrite present in the sample at that wavelength. There are hkl values for 12mm MSSS weld sample-1 as well as Iron-Nickel (Fe Ni) and ferrite iron chromium Phase present in 12mm MSSS weld sample-1

The highest peaks displayed in the spectra, which consequently find relevance in the 12mmMSSS weld sample 2 are iron and iron nickel

The second crystals measured correspond to the second peak to the right side of the highest peak on the spectra. Highest peaks displayed in the spectra, which consequently find relevance in this 12mm Stainless steel, and mild steel weld are iron nickel and manganese silicide.

Peak occurring at 45 (2θ) shows it is Austenite. The hardness decreases from the boundary of the transition zone. Chromium-Iron (Cr_{0.7} Fe_{0.3}) Phase is present in 2mm MSSS weld sample-1 and hkl values are also present for 2mm MSSS weld sample-1. Manganese-Nickel (Mn Ni₃) Phase present in 2mm MSSS weld sample-1 as well as the hkl values

3) Discussion on XRD method

XRD patterns were collected from the samples in the region of the HAZ- Fusion zone such that the

The nature of the spectrum (Sharp and definite peaks), obtained from the XRD analysis of the 12mm MSSS samples reveals a crystal-like structure unlike the amorphous nature of spectrum that is depicted by continuous wave-like peak.

Likewise, from the 12mm MSSS Sample 1, distinct phases are present such as the Iron Nickel, Iron Manganese, Chromium Iron and Chromium Nickel. In the 12mm MSSS Sample 2, we clearly see distinct phases present such as Iron and Iron Nickel. These confirms the results from the EDAX analyses of the parent metals - stainless steel and mild steel and the weld rods (filler metals) - A15 Copper filler wire and 304/316 which reveals the presence of these elements in their composition as obtained from EDAX.

The peak in the XRD figure above depicts the presence of Chromium Cr which is responsible for weld failure discussed under SEM section. [23]

From the results of the EBSD, it is obvious that there exists martensitic, ferrite and austenitic phases present in the weld samples. For the XRD analysis, the index (h, k, l) pattern was obtained and the results displayed in Table V below. The phases present were determined and their quantity as well as the crystalline size of each phase measured.

TABLE V. HKL VALUES FOR PHASES 12MM MSSS WELD SAMPLE -1 SECOND

d	2θ	l fix	h	k	l
2.02989	44.603	999	1	1	0
1.43535	64.914	115	2	0	0
1.17196	82.185	173	2	1	1
1.01495	98.744	44	2	2	0
0.9078	116.106	61	3	1	0
0.8287	136.723	16	2	2	2

The creation of Martensite consists of systematic displacement and array of atoms. This implies that austenite and Martensite will be closely interrelated which means that martensitic alterations give rise to an array of bond between parent and product lattices that can be reproduced repeatedly. Most times the Austenite and ferrite phases are parallel and as such the directions that are confirms and matches with these planes are also matching.

The Phases present in 12mm MSSS Weld Samples and their percentage (%) Quantification present the weld samples are displayed in the Table IV.

VIII. ELECTRON BACK- SCATTERING DIFFRACTION EBSD

The EBSD data were acquired using EBSD with EDAX AMETEK (OCTANE SUPER- A 1.18/195915, VERIOS/G2) Systems on a thermal field emission gun with a Four Quadrant Backscattered Electron Detector type 211/U (K.E. Developments LTD, Cambridge, England 042541); and on a tungsten source Zeiss Supra 35 VP SEM with Digi view detector. The EBSD mapping data was obtained from randomly selected 60mm² sensor area. In this very research, the EBSD analysis is used to discover the orientation of the crystals of the material (stainless steel and mild steel weld) situated inside the incident electron's beam interaction volume as well as to study the morphology and micro-texture of the specimen. Scanning the electron beam in certain manner usually hexagonal or square grid generated microstructural maps. The map generated provides details on the grain boundary the diffraction arrangement and the grain orientation. To measure the size of the grain, crystallographic and misorientation a special statistical device is used to obtain information. Misorientation is the variation in crystallographic orientation, when two crystallites located within a polycrystalline material (the HAZ of the stainless steel and mild steel) are compared.

Several plots, maps and charts are obtained from the details and information gathered. The processing history such as the residual and loading evidence after mechanical testing, the previous nature of parent material phases at elevated

temperatures; as well as the microstructural accuracy such as nature of grain boundary, the amount of microstructural information and precipitates can be obtained.

1) EBSD Approach

A well-polished sample is placed in the SEM detector at a tilt angle of 70 degrees:

1. Visual check is carried out to see that sample is parallel to the detector. The detector is positioned on the LHS in the chamber but on screen, it appears to be on the LHS in the TV mode.

2. Alignment of the image is carried out, and the entire aperture should be aligned. Approximate size is 120.0 micron (µm). High current is in Nano amperes.

3. Viewing of cross hairs, absolute direction of the SEM is along the horizontal plane.

4. Check magnification: Amperage is 0.8901 Amperes, working distance 10mm 10 11mm (not more than 13mm)

5. Scanning - sequence is from bottom to top; Right WD = 12.5. High magnification of 100

6. Scanning dynamic focussing - to make the whole picture of same degree or level. Working distance is 9.5mm, distance between beam and sample.

7. Mapping and Resolution for 100m

8. Finish and Take detector out.

Precautions Taken:

Take detector out before taking sample out to avoid detector leaks

Safest to always go back to TV mode

2) EBSD Result

The different phases present in the microstructure are Ferrite, Martensite and Austenite. For the spot 1 the phase identified is Ferrite, likewise for spot 2. For spot 3, Austenite was identified. Spots 4 and 5 are Martensite.

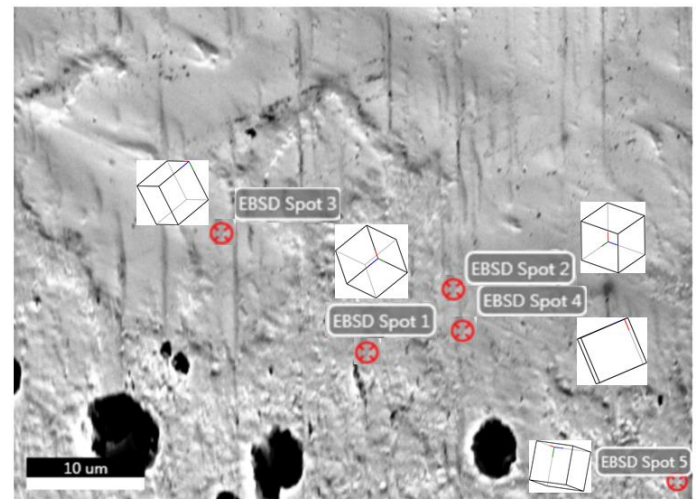
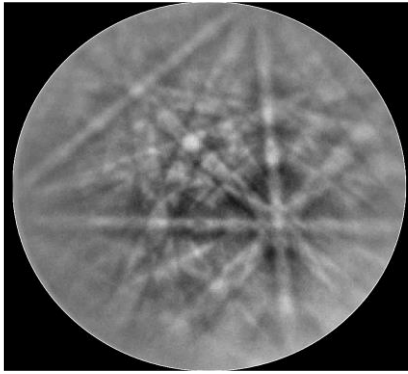


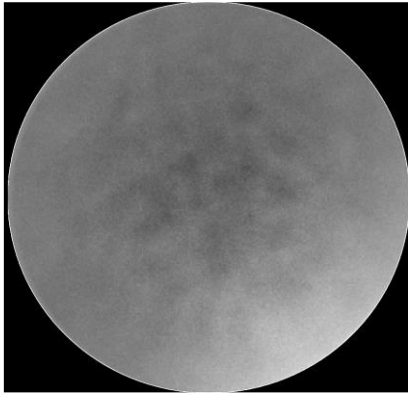
Fig. 11. Microstructure of 12mm MSSS Sample 1 showing the different phases present in the welded zone and lattice orientation of each phase - Ferrite, Austenite and Martensite.

Spots 1 and 2 have Ferrite phases present in them; Spot 3 is Austenitic in nature, while the Phases present in spot 4 and 5 are Martensite.

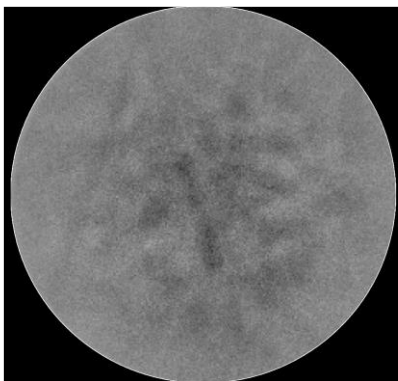
The Figure 12 (a-e) below shows the EBSD patterns obtained from the EBSD analysis. Since martensite is a body centered tetragonal (BCT) structure, depending on the quantity of carbon in it, the c/a lattice parameter varies but is approximately unity. [23] This value of the lattice parameter places Martensite as a (false) Pseudo-BCC structure and as such makes it challenging to differentiate discriminate between martensite and ferrite. Of the several EBSD patterns obtained from the samples of weld micrographs, it has been observed that the Ferrite phases had clearer structures compared with Martensite in agreement with the findings from Nowell and Wright.



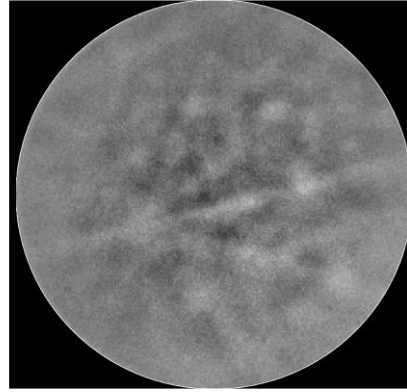
(a) Spot 1 Ferrite



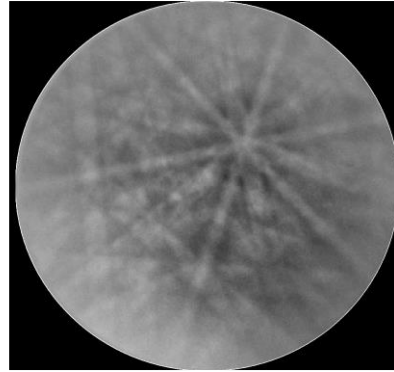
(b) Spot 2 Ferrite



(c) Spot 3 Austenite



(d) Spot 4 Martensite



(e) Spot 5 Martensite

Figure 12 (a-e) Array of the 12mm SS/MS Samples on the sample holder of the XRD detector and

3) Discussion on EBSD

There is a decrease in the hardness starting from the line of the transition zone as observed from the results of the indentation tests and micrographs. The Mo and the Mn minerals present in the welding electrodes (rods – filler metals) which increases hardness in being blended with the carbon steel and is responsible for this decrease observed in the hardness of the weld zone. The size of the grains formed in the weld metal by virtue of speedy cooling are small and fine in structure due to low heat input of the joints acquired from GMAW [20].

Depending on the phase changes present in a particular micrograph and sample, the properties of the weld also changes. The change in the orientation of the hkl values also changes the property. The presence of Martensite phase change causes a slip, break and fracture. Martensite is a mixture of Ferrite and Austenite and has loads of residual stress mass as such it is tougher.

Since there have been volumetric change and yield strength seen under tensile test curves by reason of martensitic transformation which have effects on welding residual stress, by increasing the magnitude of the residual stress in the weld zone as well as changing its sign. In agreement with the above findings, the results of the simulation [19] also reveals that the volumetric change and the yield strength change due to martensitic transformation and these have influences on the welding residual stress [23].

EBSD scan reveal presence of Ferrite, Martensite and Austenite phases. All of them are cubic structures. Ferrite is body centred cubic bcc, the crystal lattice of Martensite is a body-centred tetragonal form of iron in which some carbon is dissolved whereas Austenite is face centred.

IX. SOME ASPECTS IN NUMERICAL APPROACH

1) Weld direction - nomenclature

The usual concept of 90 degrees, 180 degrees, 270 degrees and 360 degrees has been used in a clockwise manner to describe the direction of the weld, as well as the 3 o'clock, 6 o'clock, 9 o'clock and 12 o'clock convention.

Figure 13 illustrates the 45, 135, 225 and 315-degree reference system, which is obtained by simply rotating the cross-section of the pipe in Figure 1 through an angle of 45 degrees in the clockwise direction.

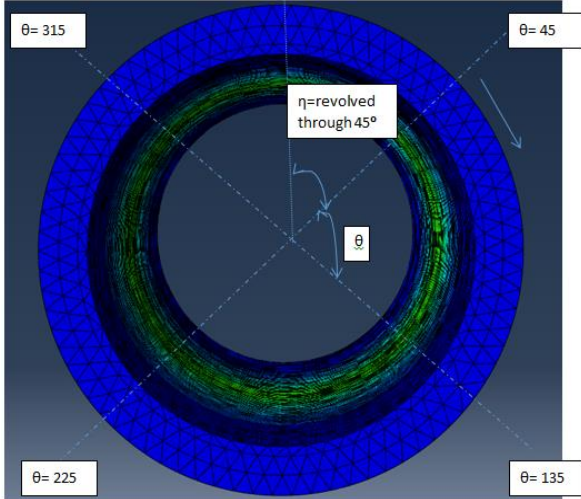


Fig. 13. A representation of the pipe rotation and nomenclature of 45, 135, 225 and 315 degrees

The above style of representation of a welding direction is known as 1:30 hours, 4:30 hours, 7:30 hours and 10:30 hours face of a clock using a temporal connotation. Representing the four positions of interest on the pipe circumference onto a plate, following the Gaussian transformation principle, the weld direction can also be obtained [19]. This implies that different weld directions can also be represented on a plane surface as shown on the 2D plate. [19]

2) Thermal Analysis

From the different plots of temperature versus distance, the effect of the clad on the weld is such that the clad has effectively reduced the operating temperature thereby limiting the thermal conductivity of the welded path. The reduction in thermal conductivity enhances the insulating effect of the cladding [19].

The thermal diffusivity varies directly with the density and specific heat of the material. This implies that, as the thickness of the insulating material increases, the thermal diffusivity reduces. The material density is directly related to the insulation performance.

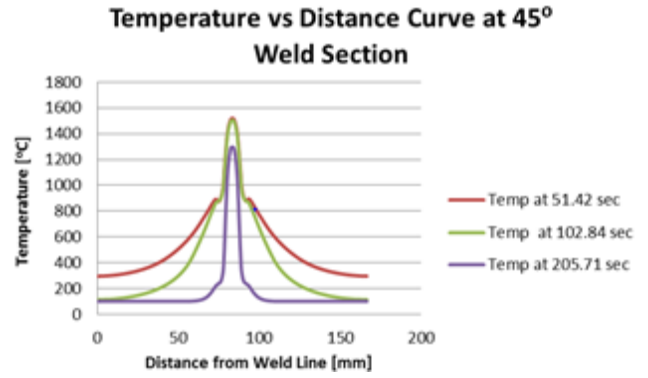


Fig. 14. Axial temperature distributions for 45° cross-section at different weld times from the weld start

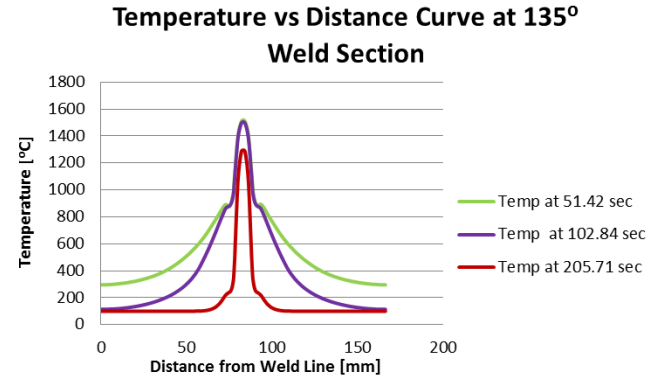


Fig. 15. Axial temperature distributions for 135° cross-section at different weld times from the weld start

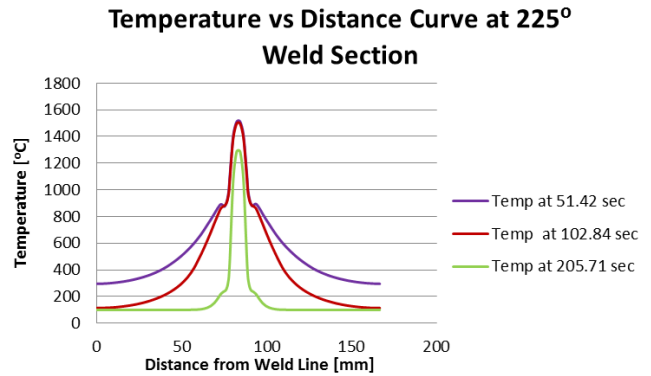


Fig. 16. Axial temperature distributions for 225° cross-section at different weld times from the weld start

Bearing in mind that the temperature imparts directly on the toughness, modulus of elasticity, ultimate tensile strength and yield stress, this means that an increased operating temperature will also impact upon these properties of the clad pipes.

3) Stress Analysis

From Figures 17, which display the residual axial stress in the clad pipe, close to the weld vicinity, compressive and tensile stress fields are present in and near the section of the weld both on the external and internal surfaces of the pipe. [19] Furthermore, this occurrence can be credited to the varying temperature profiles on the inner and outer surfaces of the pipe. By virtue of the thickness of the cylinder wall and being very close to the weld line (which is represented by the vertical line), tensile and compressive residual stress fields are generated due to shrinkage occurring within the weld pipe [5] [20] and [24].

The differences in the values of the residual stresses are a result of the different material properties such as yield strength for the base and filler metals, weld geometry and heat source parameters. There have been volumetric change and yield strength as a result of martensitic transformation, which have effects on welding residual stress, by increasing the magnitude of the residual stress in the weld zone as well as changing its sign. The simulated results show that the volumetric change and the yield strength change due to the martensitic transformation have influences on the welding residual stress.



Fig. 17. Welded plates showing residual tensile stress (underneath - inside pipe) and compressive stress (above - outer surface of pipe).

4) Radial Shrinkage

When the weldment cools down, there is usually an axial inclination of the constraint free end of the pipe taking place. The thickness of the pipe is considered for the radial shrinkage and measured for four different increments, so that the shrinkage in thickness could be appreciated. At a tilt angle of 45 degrees, the radial shrinkage is 0.022mm, and similarly at an angle of 27.5 degrees, the radial shrinkage is 0.010mm. [19]

5) Axial Shrinkage

For four different increments of the axial length, the shrinkage is measured and plotted against the normalized distance from the weld path. The axial shrinkage at lower increments is slightly different from those at higher increments, because there are high thermal gradients experienced during Butt welding leading to residual stress and discrepancy in hardness, hence a creep effect is observed at higher increments. [19]

X. CONCLUSION

From the various plots of temperature versus distance along the path of weld propagation, it has been observed that the distribution of heat follows a unique pattern which has been displayed in Figures 14 to 16, with the different HAZ being considered. The peaks displayed in the plots correspond to the immediate vicinity of the weld, with the number and magnitude of the peaks increasing as the cumulative quantity of heat is dispelled within the weldment, and likewise decreasing the further away one goes from the region of the weld.

It is significant to note that there exists a linear relationship between the tensile strength and the hardness of the weld and consequently, the ultimate tensile test. From the results of the simulated axial stress and the residual axial stress distributions on the inner surface of the pipe, as well as the XRD, EBSD and hardness, the following can be deduced

1. There is a decrease in the hardness starting from the line of the transition zone as observed from the results of the indentation tests and micrographs.

2. The Mo and the Mn minerals present in the welding electrodes (rods – filler metals) which increases hardness in being blended with the carbon steel and is responsible for this decrease observed in the hardness of the weld zone.
3. The size of the grains formed in the weld metal by virtue of speedy cooling are small and fine in structure due to low heat input of the joints acquired from GMAW.
4. The properties of the weld also change depending on the phase change present in a particular micrograph and sample.
5. The Hardness in the FZ and HAZ is 30-70% more than that in the Parent material
6. Linear relationship exists between the Yield stress and the Hardness of the weld samples which further confirm for the 12mm stainless steel clad that the value of hardness increases with the decrease in temperature and applied load.
7. There is a similar trend in the increased tensile profile across the fusion zone and HAZ
8. The hardness of the HAZ varies linearly from the clad/HAZ interface to the HAZ/baseline interface with values 200Hv to 330Hv accordingly.
9. The reason for the direct variation of hardness in the HAZ is the difference in heating temperature in the HAZ resulting in variation in the growth of grain.
10. Close to the region of weld region, comprehensive axial, radial and hoop stresses can be observed but farther away from the weld region, tensile stresses become the trend.
11. Also, due to the symmetry across the weld line W_L , the axial stresses are symmetric in nature.
12. The radial and axial shrinkage effects on the 12mm clad pipe also agree with findings from the thermal analysis, tensile stress curve and microstructures of weld.
13. Results from the literature further confirm the validity of the simulations carried out in this research.

The XRD pattern is used to confirm that the XRD pattern in the HAZ area is similar to that of the bulk material – parent material (stainless steel and mild steel as well as filler metals (316/304 and A15 Copper wire). The microstructure although similar, cannot be the same because of the cooling conditions.

ACKNOWLEDGMENT

The authors sincerely express their gratitude to IEANG and WCE for the great privilege to be awarded Best Paper Publication at the WCE 2017 Conference and for the opportunity to publish this paper as an IAENG publication in the Special issue of Engineering Letters.

The authors want to express their gratitude to Brunel University London for the facilities provided and conducive research environment.

The first author also thanks The Petroleum Technology Development Fund (PTDF) for their funding and support through which this research has been made possible.

REFERENCES

- [1] S. Lampman, "Weld Integrity and Performance", ASM International, 2001.
- [2] J.A. Goldak, "Computational Welding Mechanics", Springer, 2005
- [3] A.G. Youtsos, "Residual Stress and its Effects on Fatigue and Fracture", Springer, 2006
- [4] E. Muhammad, "Analysis of Residual Stresses and Distortions in Circumferentially Welded Thin-Walled Cylinders", National University of Science and Technology, Pakistan, 2008.
- [5] N.U. Dar, E.M. Qureshi and M.M.I. Hammouda, "Analysis of weld-induced residual stresses and distortions in thin-walled cylinders", Journal of Mechanical Science and Technology, Vol. 23, pp. 1118-1131, 2009.
- [6] M.E. EDU, "Gaussian Curvature", retrieved from Math ETSU EDU, December 29, 2016.
- [7] C.P. Stone, P. Omnes, R.V.P Rezende, H. Grimm-Strele and R.E Bensow, www.researchgate.net: https://www.researchgate.net/post/Can_somebody_outline_the_advantages_of_utilizing_a_hexahedral_mesh_as_compared_to_a_tetrahedral_mesh2 retrieved September 12, 2016.
- [8] Struers. *Grinding and Polishing* . Retrieved from Struers Ensuring Certainty: www.struers.com, 2018
- [9] Struers. *Metallography of Welds*. Retrieved from Struers: www.struers.com, 2018
- [10] G. F. Vander Voort, *Metallography of Welds*. Retrieved from Advanced Materials and Processing: www.asminternational.org 2011
- [11] S. A. Technologies, *Iron-Carbon Phase Diagram*. Retrieved 07 09, 2016, from SubsTech: http://www.substech.com/dokuwiki/doku.php?id=iron-carbon_phase_diagram, 2012
- [12] J. T. Busby, M. C. Hash and G. S. Was. The Relationship between Hardness and Yield Stress in Irradiated Austenitic and Ferritic Steels. *Journal of Nuclear Materials* , 267-278, 2004.
- [13] M. N. Gusev, O. P. Maksimkin, O. V. Tivanova, N. S. Silnaygina and F. A. Garner. Correlation of yield stress and microhardness in 08Cr16Ni11Mo3 stainless steel irradiated to high dose in the BN-350 fast reactor. *Journal of Nuclear Materials*, volume 359, 258-262, 2006.
- [14] C. A. Sila, J. Teixeira de Assis, S. Phillippov and J. P. Farias. Residual Stress, Microstructure and Hardness of Thin-Walled Low-Carbon Steel Pipes Welded Manually. *Materials Research*, 1-11., 2016.
- [15] W. Suder, A. Steuwer and T. Pirlin . Welding Process Impact on Residual Stress Distortion. *Science and Technology of Welding and Joining*, 1-21, 2009.
- [16] G. Benghalia and J. Wood Material and Residual Stress Considerations Associated with the Autofrettage of Weld Clad Components. *International Journal of Pressure Vessels and Piping*, 1-13, 2016.
- [17] D.S. Sun, Q. Liu, M. Brandt, M. Janardhana and G. Clark, "Microstructure and Mechanical Properties of Laser Cladding Repair of AISI 4340 Steel", International Congress of the Aeronautical Sciences, pp. 1-9, 2012.
- [18] N. Mathiazhagan, K. Senthil, V. Balasubramanian and V. C. Sathish Gandhi. Performance Study of Medium Carbon Steel and Austenitic Stainless Steel Joints: Friction Welding. *Oxidation Communication*, 2123-2134. (2015)
- [19] B. Kogo., B. Wang, L. Wrobel, and M. Chizari, Residual Stress Simulations of Girth Welding in Subsea Pipelines. *World Congress on Engineering 2017* (pp. 861-866). London U.K.: World Congress on Engineering (2017).
- [20] P.K. Sinha, R. Islam, C. Prasad and M. Kaleem, "Analysis of residual stresses and distortions in girth-welded Carbon steel.
- [21] T. Kursun, Effect of the GMAW and the GMAW-P Welding Processes on the Microstructure. *Archives of Metallurgy and Materials Vol 56*, pp. 995-963, 2011.
- [22] A. K. Lakshminarayanan and V. Balasubramanian, An Assessment of Microstructure Hardness Tensile and Impact Strength of Friction Stir Welded Ferritic Satainless Steel Joints. *Materials and Design 31*, 4592-4600, 2010.
- [23] M. Nowell and S. I. Wright, Differentiating Ferrite and Martensite in Steel Microstructures Using Electron Backscatter Diffraction. *ResearchGate*, 1-12, 2009.
- [24] D. Dean and M. Hidekazu, Prediction of Welding Residual Stress in Multi-Pass Butt-Welded Modified 9Cr-1Mo Steel Pipe Considering Phase Transformation Effects. *Comput. Mater. Sci*, 37, 209–219, 2006.